Materials Science & Engineering C 111 (2020) 110765

Contents lists available at ScienceDirect

Materials Science & Engineering C

journal homepage: www.elsevier.com/locate/msec

Unveiling the role of β-Ag_2MoO_4 microcrystals to the improvement of antibacterial activity

Camila Cristina De Foggi[a,*], Regiane Cristina De Oliveira[b], Marcelo Assis[b], Maria Tereza Fabbro[b], Valmor Roberto Mastelaro[c], Carlos Eduardo Vergani[a], Lourdes Gracia[d], Juan Andrés[d], Elson Longo[b], Ana Lucia Machado[a]

[a] São Paulo State University (UNESP), Department of Dental Materials and Prosthodontics, 14801-907, Brazil
[b] Interdisciplinary Laboratory of Electrochemistry and Ceramics, University Federal of São Carlos, P.O. Box 676, 13565-905 São Carlos, SP, Brazil
[c] São Carlos Institute of Physics, University of São Paulo, CP 369, São Carlos 13560-970, São Paulo, Brazil
[d] Department of Physic and Analytical Chemistry, Universitat Jaume I, Campus Riu Sec, E-12071 Castellón, Spain

ARTICLE INFO

Keywords:
β-Ag_2MoO_4
Antibacterial activity
Morphology evolution

ABSTRACT

Crystal morphology with different surfaces is important for improving the antibacterial activity of materials. In this experimental and theoretical study, the antibacterial activity of β-Ag_2MoO_4 microcrystals against the Gram-positive bacteria, namely, methicillin-resistant *Staphylococcus aureus* (MRSA), and the Gram-negative bacteria, namely, *Escherichia coli* (*E. coli*), was investigated. In this study, β-Ag_2MoO_4 crystals with different morphologies were synthetized by a simple co-precipitation method using three different solvents. The antimicrobial efficacy of the obtained microcrystals against both bacteria increased according to the solvent used in the following order: water < ammonia < ethanol.

Supported by experimental evidence, a correlation between morphology, surface energy, and antibacterial performance was established. By using the theoretical Wulff construction, which was obtained by means of density functional calculations, the morphologies with large exposition of the (001) surface exhibited superior antibacterial activity. This study provides a low cost route for synthesizing β-Ag_2MoO_4 crystals and a guideline for enhancing the biological effect of biocides on pathogenic bacteria by the morphological modulation.

1. Introduction

Metal molybdates such as A_xMoO_z (where A is a monovalent, divalent, or trivalent metal ion) have recently been investigated intensively [1–14] owing to their chemical stability and unique crystal structure (layers of molybdenum oxide octahedra separated by the metal ions) [15], which make them suitable for a wide range of applications. Particularly, silver molybdates have been investigated in the fields of lubrication [16,17], humidity and gas sensors [18,19], photoelectronic devices [6], surface enhanced Raman scattering techniques [20,21], photocatalysis [3,4,15,22–30], and photoluminescence [22,31,32]. Several synthesis methods have been reported, such as hydrothermal [21,33–36], solution-based chemical reaction [20], co-precipitation [4,25,26,32,37,38], dynamic template route [23], laser annealing [39], and microwave-assisted hydrothermal methods [22,24,40,41]. In this context, Ng and Fan [42] have recently reported the preparation of β-Ag_2MoO_4 crystals with high-index facets *via* the delicate tuning of the supersaturation conditions during crystal growth. Additionally, they were able to find a relationship between morphology and photocatalytic activity.

The morphological modulations can be achieved by the different solvents (water, ammonia, and ethanol) used in the co-precipitation synthesis method, as we described previously [37].

As a continuation of our work in this field of research, in this paper, we report the antibacterial activity of β-Ag_2MoO_4 microcrystals against gram-positive bacteria, namely, methicillin-resistant *Staphylococcus aureus* (MRSA), and gram-negative bacteria, namely, *Escherichia coli* (*E. coli*). These bacteria are important because they are opportunistic pathogens that are often inherently resistant to antibiotics or capable of rapidly building resistance to many common antimicrobial agents [43]. More significantly, the biological effects of β-Ag_2MoO_4 with different morphologies on the bacteria are systematically discussed. Additionally, to gain a deeper understanding of the atomic and electronic structure, and to establish a correlation among the morphology, surface energy, optical properties, and antibacterial activities, we conducted first principle calculations on the basis of density functional theory

* Corresponding author.
E-mail address: camilafoggi@gmail.com (C.C. De Foggi).

https://doi.org/10.1016/j.msec.2020.110765
Received 10 September 2018; Received in revised form 14 January 2020; Accepted 18 February 2020
Available online 20 February 2020
0928-4931/

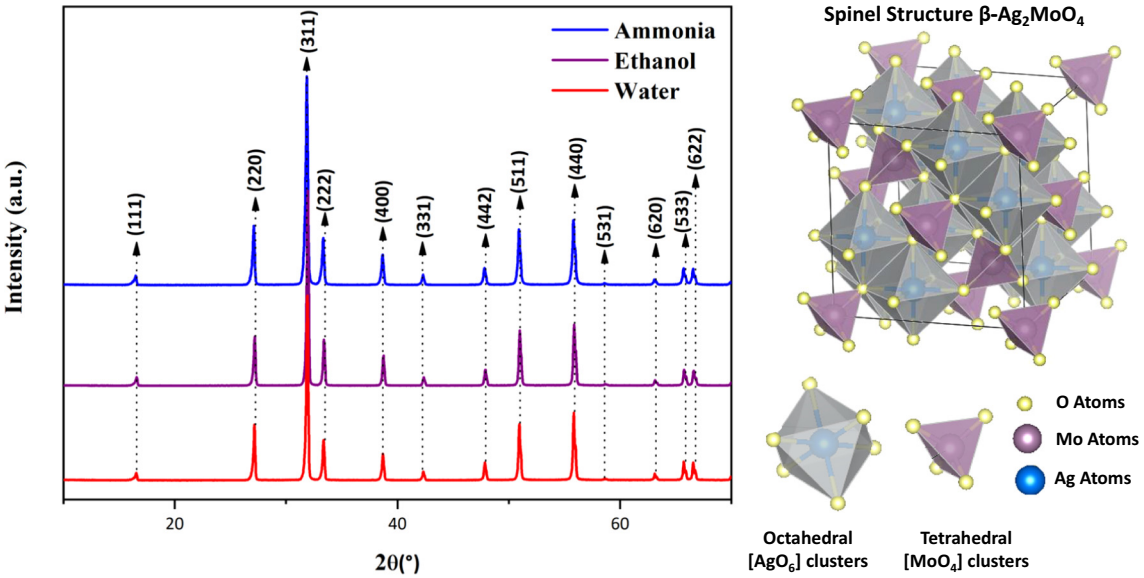

Fig. 1. XRD patterns of the β-Ag_2MoO_4 microcrystals synthesized in water, ethanol and ammonia.

(DFT) to complement our experimental findings. This study intends to provide a more comprehensive insight into the development of novel biocide with a unique morphology and future potential for use in biological applications.

2. Results and discussion

The β-Ag_2MoO_4 microcrystals were synthesized by using different solvents (water, ammonia, and ethanol) and the co-precipitation method. The experimental method is described in the Supplementary Material (SM) section. The samples were structurally characterized by x-ray (XRD) diffraction to evaluate the order/disorder at long range. Fig. 1 shows the XRD for the samples of silver molybdate. It was observed that all compounds presented a structure type assigned to a cubic spinel with the Fd3m space group, which is in agreement with the *Inorganic Crystal Structure Database* (ICSD) card 238,013 [22]. The lattice parameters for the β-Ag_2MoO_4 phase are a = b = c = 9.3170 Å and a = b = c 90°. Moreover, Fig. 1 shows clearly that there was no other additional peak; that is, there was no undesirable secondary phase. Fig. 1 shows the cubic spinel structure type that was composed by distorted octahedral clusters [AgO_6] with Oh symmetry for the Ag sites, and distorted tetrahedral clusters [MoO_4] with Td symmetry for the Mo sites. The crystallinity degree of a structure (order/disorder), that is, the organization at long range is directly dependent of the manner of the ions organize themselves into the structure, being that it is totally dependent on the chemical environment in which the material is formed. Therefore, the change of solvent, or the addition of any species in the synthesis of the material may corroborate a change in the order/disorder. A factor related to structural order/disorder effects at long-range can be found by the analysis of the full width at half maximum (FWHM) of the most intense peak of the XRD patterns, related to the plane (311) of the β-Ag_2MoO_4. The samples obtained in water, ethanol and ammonia, have FMHW values of 0.18, 0.21 and 0.23° respectively, showing that the samples synthesized with ethanol and ammonia have a lower degree of order than the samples obtained in water.

Raman spectroscopy is a technique complementary to XRD for estimating structural order/disorder at short-range. Fig. 2 shows the experimental spectra obtained for all samples. The β-Ag_2MoO_4 belongs to the point-group symmetry O_h^7 with the centrosymmetric inversion, which indicates five active Raman modes (A_{1g}, E_g, and T_{2g}) obtained from the decomposition of point Γ (Γ = A_{1g} + E_g + 3T_{2g} + T_{1g}) [22]. Fig. 2a shows the spectra for the samples obtained in different solvents. The spectra of all samples show four characteristic peaks centered at 276, 355, 761, and 873 cm^{-1}. The first Raman mode at 276 cm^{-1} is associated with a transition E_g, which refers to external structure vibrations on the [AgO_6] clusters [22]. The Raman mode at 355 cm^{-1} was associated with the transition T_{2g} caused by the O—Mo—O asymmetric bending vibrations [22,44]. Both the 761 and 873 cm^{-1} modes are associated with the T_{2g} and A_{1g} transitions, respectively, and were caused by the asymmetric and symmetric O—Mo—O vibrations [22,44]. Fig. 2b shows shows FT-IR for the samples of β-Ag_2MoO_4. In the FT-IR spectra of the samples the band at 827 cm^{-1} is observed related to an asymmetrical stretching of the O—Mo—O bonds of the [MoO_4] tetrahedral clusters [3,45]. Other vibrations are not observed because they appear below 400 cm^{-1}, outside the limit of the equipment used.

Theoretical investigations based on first principle calculations by *ab-initio* and quantum-chemical simulations have been increasingly used to complement the experimental findings, provide valuable information of the electronic, structural, and energetic properties, and simulate and predict the morphology of the materials [22,44,46]. Thus, by using this combined experimental and theoretical approach, previous studies determined that the most stable morphology for the β-Ag_2MoO_4 can occur when the surface energies are 1.90,1.28, and 3.46 J/m^2 for the (001), (011), and (111) faces, respectively [37,44].

Considering that Ag_2MoO_4 acquires different morphologies according to the synthetic method employed [37,40], in this study, the morphologies of the β-Ag_2MoO_4 samples were investigated by field emission scanning electron microscopy (FE-SEM), and are of fundamental importance to understanding the morphological evolution process and changes in the surfaces of the crystals with the variations of the used solvents. The β-Ag_2MoO_4 samples that were obtained by using different solvents are shown in Fig. 3. The predominant morphologies obtained experimentally display the exposed (001), (011), and (111) surfaces, which support the hypothesis that these surfaces are stabilized by interacting with the solvent molecules. This observation suggests that the Wulff shape of β-Ag_2MoO_4 is closely related to the chemical environment. FE-SEM additional images are showed in the SM (Fig. S1).

For the following discussion on the relationship between the morphology-antibacterial activity of the β-Ag_2MoO_4 samples to be valid, it is assumed that the structure and facet composition of the crystals are preserved in the time scale of the experiments. The Wulff crystal representation of the optimized β-Ag_2MoO_4, and the available morphologies that would be obtained by assuming different values for the

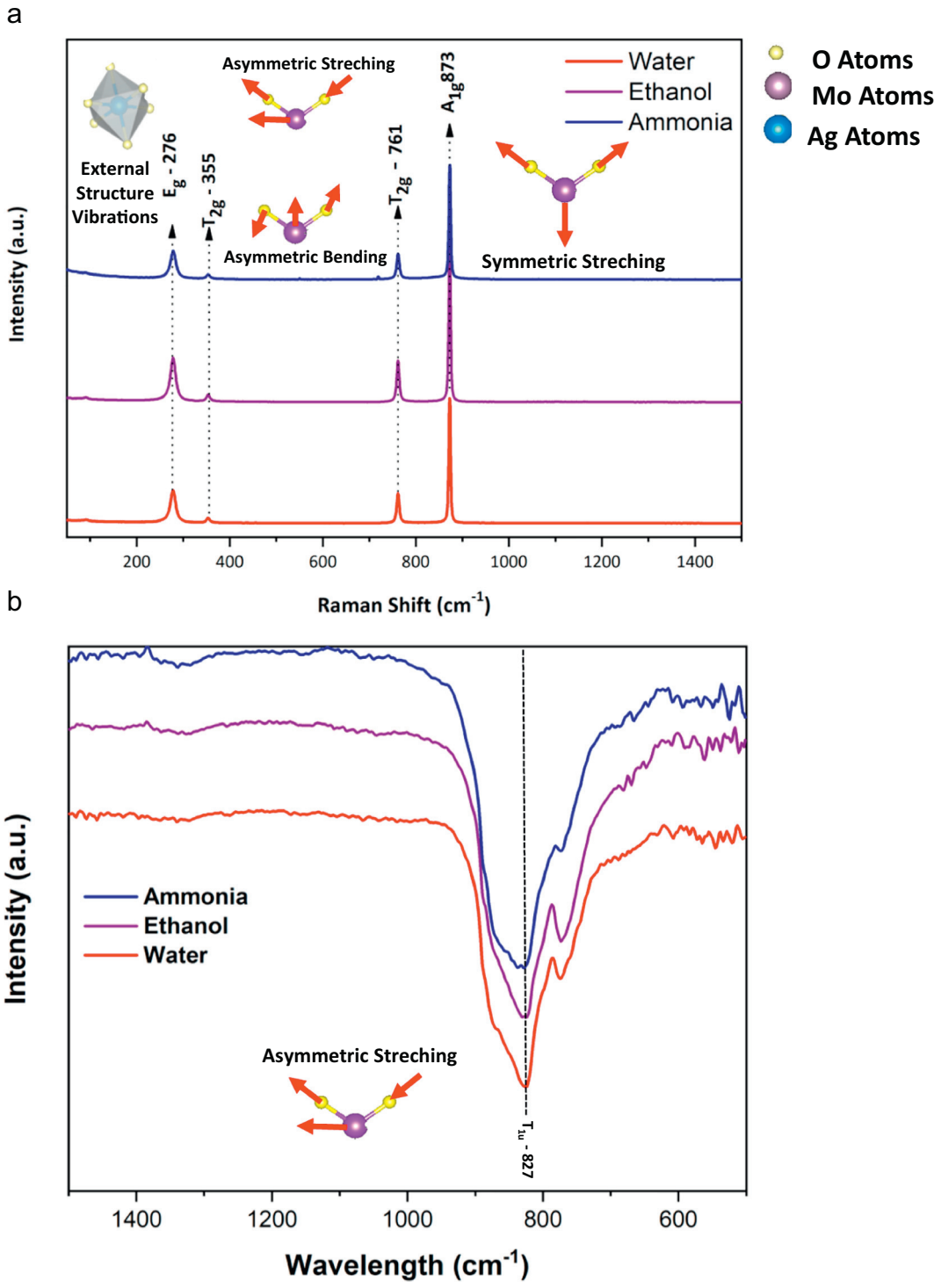

Fig. 2. Raman (2a) and FT-IR (2b) spectra of the β-Ag_2MoO_4 microcrystals synthesized in water, ethanol and ammonia.

surface energies of the three facets are displayed in Fig. 4. By analyzing Fig. 4, it can be seen that the experimental and theoretical morphologies are in good agreement: (a) when water was used as the solvent, the surface energy of the (111) surface decreased from 3.46 to 1.28 J/m^2; (b) when ammonia was used as the solvent; the surface energy of the (111) surface decreased from 3.46 to 1.28 J/m^2, and the surface energy of the (001) surface decreased from 1.90 to 1.5 J/m^2; (c) when ethanol was used as the solvent, the surface energy values of both the (111) and (001) surfaces decreased to 1.28 J/m^2.

The minimum inhibitory concentrations (MICs), which are defined as the lowest concentrations required for complete growth inhibition (no visible growth by visual inspection), and the minimum bacterial concentrations (MBCs), which are defined as the lowest concentrations that do not result in bacterial growth on plates, were determined for the β-Ag_2MoO_4 microcrystals that were synthesized in different solvents (water, ammonia, and ethanol). The tests were performed according to the standard methods described in Clinical Laboratory Standards Institute (CLSI) [47]. The microorganisms evaluated in this study were MRSA (ATCC 33591) and *E. coli* (ATCC 8739). In the microbiological test results shown in Fig. 5, the MIC value was the same as the MBC

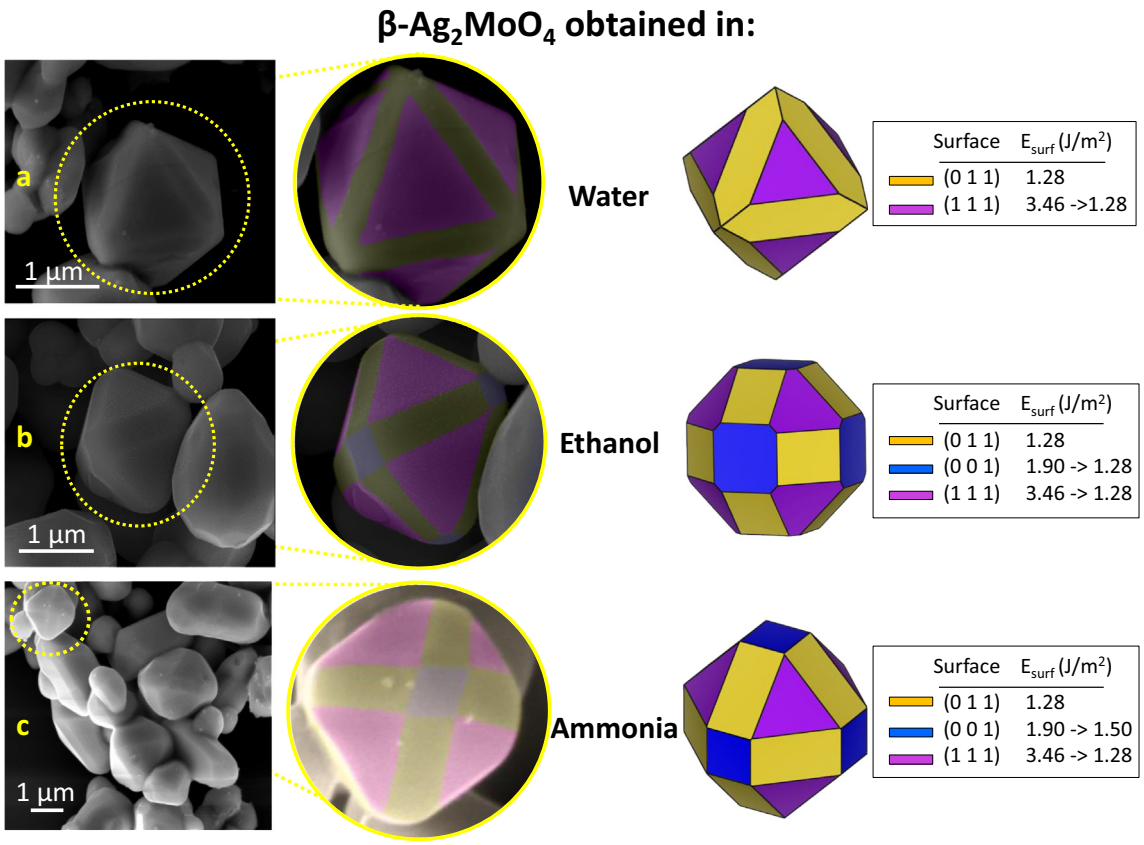

Fig. 3. FE-SEM images, morphologies, and facets of the β-Ag_2MoO_4 samples obtained by using different solvents: (a) water, (b) ethanol, and (c) ammonia.

value for MRSA for the three solvents used in the synthesis of the β-Ag_2MoO_4. Similar findings were observed for *E. coli*.

When the microcrystals were synthesized with ethanol, the MIC/MBC value (31.25 μg/mL) for MRSA was lower than that observed for the microcrystals synthesized with ammonia (62.50 μg/mL). Additionally, the bactericidal activity of both β-Ag_2MoO_4 microcrystals was higher than that exhibited by the samples synthesized in water, which required higher concentration (250 μg/mL) to inhibit the MRSA growth. Fig. 5a shows that, in comparison with the control (8.8 ± 0.71 $\log_{10}$ CFU/mL), at half of the MICs/MBCs values, the MRSA growth was reduced by approximately 4 logs for the β-Ag_2MoO_4 microcrystals synthesized by using ethanol (to 4.3 ± 0.07 $\log_{10}$ CFU/mL), 5 logs for the microcrystals synthesized in ammonia (to 3.9 ± 0.06 $\log_{10}$ CFU/mL), and 4 logs when water was used as the solvent (to 4.3 ± 0.07 $\log_{10}$ CFU/mL).

For *E. coli*, the microcrystals synthesized using ethanol exhibited a lower MIC/MBC value (0.49 μg/mL) than that observed for the microcrystals synthesized in ammonia (1.95 μg/mL) and water (3.91 μg/mL). The incubation of the bacteria in the presence of half of the microcrystal MICs produced a reduction of growth of approximately 5 logs for the β-Ag_2MoO_4 microcrystals, in comparison with the control (7.3 ± 0.20 $\log_{10}$ CFU/mL) and regardless of the solvent used in the synthesis (Fig. 5b).

Oliveira et al. found different morphologies of Ag_2MoO_4 according to the synthesis used. When ethanol was employed, there was improvement in its antibacterial activity against the same *E. coli* strain [40]. In this study, in addition to observing better anti-*E. coli* activity for the sample synthesized in ethanol, we also tested, for the first time, the efficiency against MRSA, which is a highly pathogenic bacterium.

It is worth noting that, for the three β-Ag_2MoO_4 microcrystals obtained in water, ammonia, and ethanol, the concentrations required to kill *E. coli* were always significantly lower than those required to kill MRSA. These findings can be attributed, at least in part, to the different cell wall structures. The Gram positive bacteria, namely, MRSA are composed of a cytoplasmic membrane and a thick, overlying peptidoglycan network (10–40 nm) composed of repeating units of a disaccharide-multipeptide building block that are polymerized and cross-linked to create a continuous network that envelops the cell [48]. This peptidoglycan network has several layers and contains mainly carboxyl, amide and hydroxyl functional groups [49], and teichoic acids (TAs). Two distinct types of TAs have been identified: wall teichoic acids (WTAs) that are linked to and embedded into the peptidoglycan, and lipoteichoic acids (LTAs) extending into and anchored to the cell membrane (cytoplasmatic membrane) [50]. On the contrary, TAs were not found in gram-negative bacterial cells, such as *E. coli* [49,50]. Additionally, although gram-negative bacteria contain an outer membrane, they only have a single peptidoglycan layer that is thin (3–6 nm) and located in the periplasmatic space between the outer membrane and the inner (cytoplasmatic) membrane [48]. Given that the cell wall is crucial to the mechanical and chemical integrity of the cells, because it protects them from the external environment and stress, all the mentioned differences between the gram-positive and gram-negative bacteria may have contributed to the higher activity of the synthesized β-Ag_2MoO_4 microcrystals against *E. coli*, in comparison to MRSA.

From Fig. 6a, b, and c, we can see that the (111) surfaces of β-Ag_2MoO_4 were Mo, O, and Ag ion-terminated, while the (001) and (011) surfaces were O– and Ag ion-terminated. In the (111) surface, the Ag cations were coordinated to three oxygen anions to form [AgO_3. $3V_O^x$] complex clusters, and the Mo cations were coordinated to only one oxygen anion (disfavoring its stability). The (011) surfaces exhibited the Ag cations surrounded by four oxygen anions, which resulted in the [AgO_4. $2V_O^x$] complex clusters, while in the (001) surfaces, the silver cations were coordinated to five oxygen anions and formed [AgO_5. V_O^x] complex clusters (more stable for the electron/hole recombination processes). In addition to the atomic configuration of the exposed facets, the solvent used in the synthesis had a great effect on

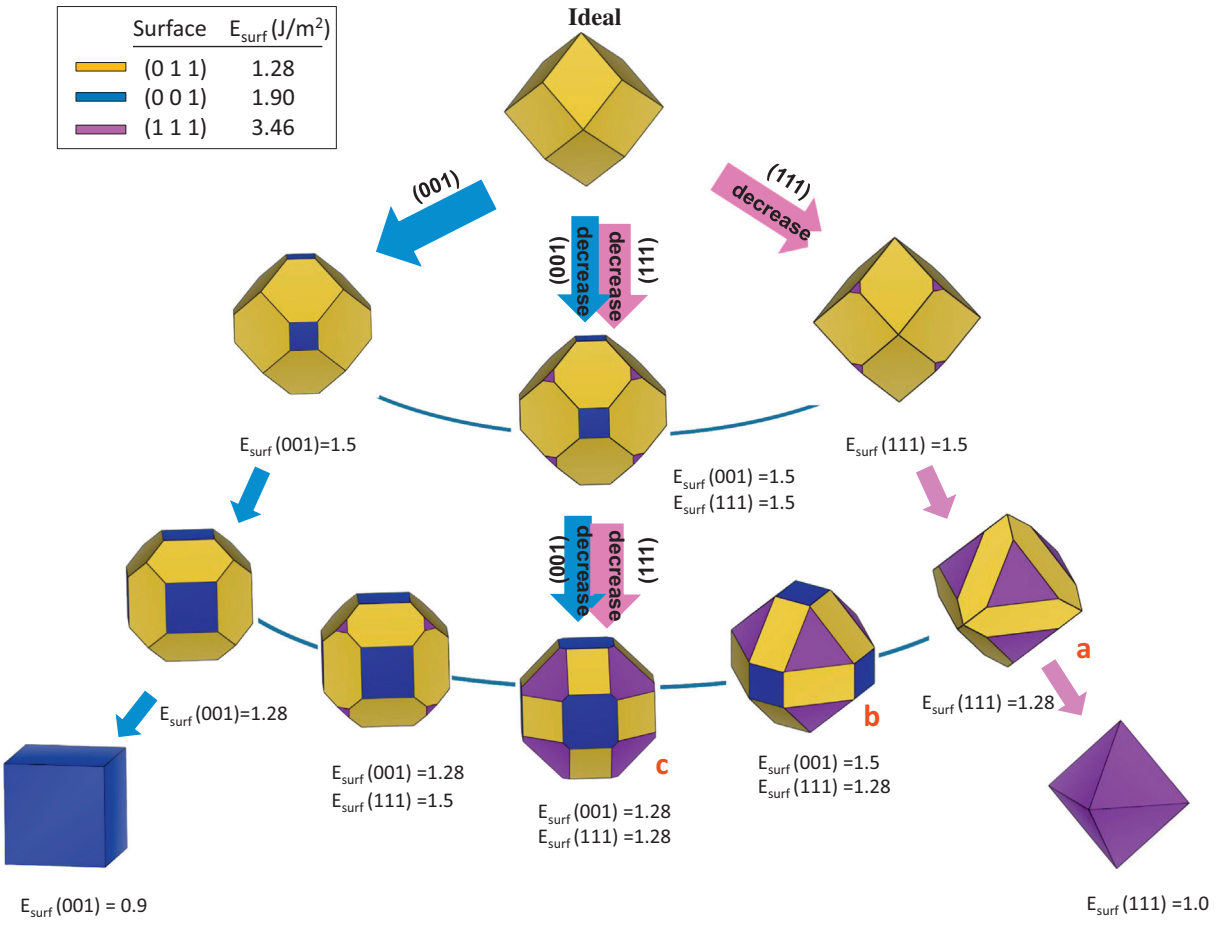

Fig. 4. Map of available β-Ag_2MoO_4 morphologies based on Wulff crystal construction as function of surface energy values.

the reactivity and stabilization of the surfaces.

A semi conductor's antibacterial activity mechanism is mainly attributed to the oxidative stress caused by the OH*, O_2', and O_2H* (reactive species) in contact with the bacterial cell wall [51,52], when $[AgO_3.\ 3V_O^{x}]$, $[AgO_4.\ 2V_O^{x}]$, $[AgO_5.\ V_O^{x}]$, $[AgO_6]^{x}$,and $[MoO_4]_o^{x}$ complex clusters, from which the β-Ag_2MoO_4 semiconductor is formed, are excited (Eqs. (1)-(7)).

$$[MoO_4]_o^{x} + [MoO_4]_d^{x} \rightarrow [MoO_4]_o' + [MoO_4]_d^{\bullet}. \quad (1)$$

$$[AgO_6]^{x} + [AgO_5V_O^{x}] \rightarrow [AgO_6]' + [AgO_5V_O^{\bullet}]. \quad (2)$$

$$[AgO_6]^{x} + [AgO_5V_O^{\bullet}] \rightarrow [AgO_6]' + [AgO_5V_O^{\bullet\bullet}]. \quad (3)$$

$$[AgO_6]^{x} + [AgO_4V_O^{x}V_O^{x}] \rightarrow [AgO_6]' + [AgO_4V_O^{x}V_O^{\bullet}]. \quad (4)$$

$$[AgO_6]^{x} + [AgO_4V_O^{x}V_O^{\bullet}] \rightarrow [AgO_6]' + [AgO_4V_O^{x}V_O^{\bullet\bullet}]. \quad (5)$$

$$2[AgO_6]^{x} + [AgO_3V_O^{x}V_O^{x}V_O^{x}] \rightarrow 2[AgO_6]' + [AgO_3V_O^{x}V_O^{\bullet}V_O^{\bullet}]. \quad (6)$$

$$2[AgO_6]^{x} + [AgO_3V_O^{x}V_O^{\bullet}V_O^{\bullet}] \rightarrow 2[AgO_6]' + [AgO_3V_O^{\bullet}V_O^{\bullet}V_O^{\bullet\bullet}]. \quad (7)$$

The $[AgO_5V_O^{\bullet}]$, $[AgO_5V_O^{\bullet\bullet}]$, $[AgO_4V_O^{x}V_O^{\bullet}]$, $[AgO_4V_O^{x}V_O^{\bullet\bullet}]$, $[AgO_3V_O^{x}V_O^{\bullet}V_O^{\bullet}]$, and $[AgO_3V_O^{\bullet}V_O^{\bullet}V_O^{\bullet\bullet}]$ complex clusters transfer a

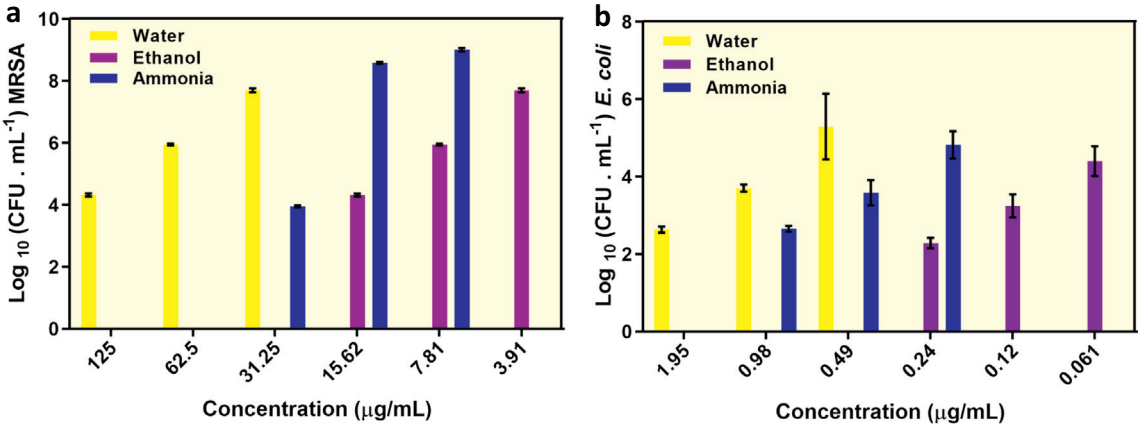

Fig. 5. Summary of $\log_{10}$ CFU/mL MRSA values (a) and *E. coli* (b) obtained for sub-inhibitory concentrations of the β-Ag_2MoO_4synthesized in water, ammonia, and ethanol. Control MRSA = 8.8 (± 0.71) $\log_{10}$ CFU/mL; control *E. coli* = 7.3 (± 0.20) $\log_{10}$ CFU/mL.

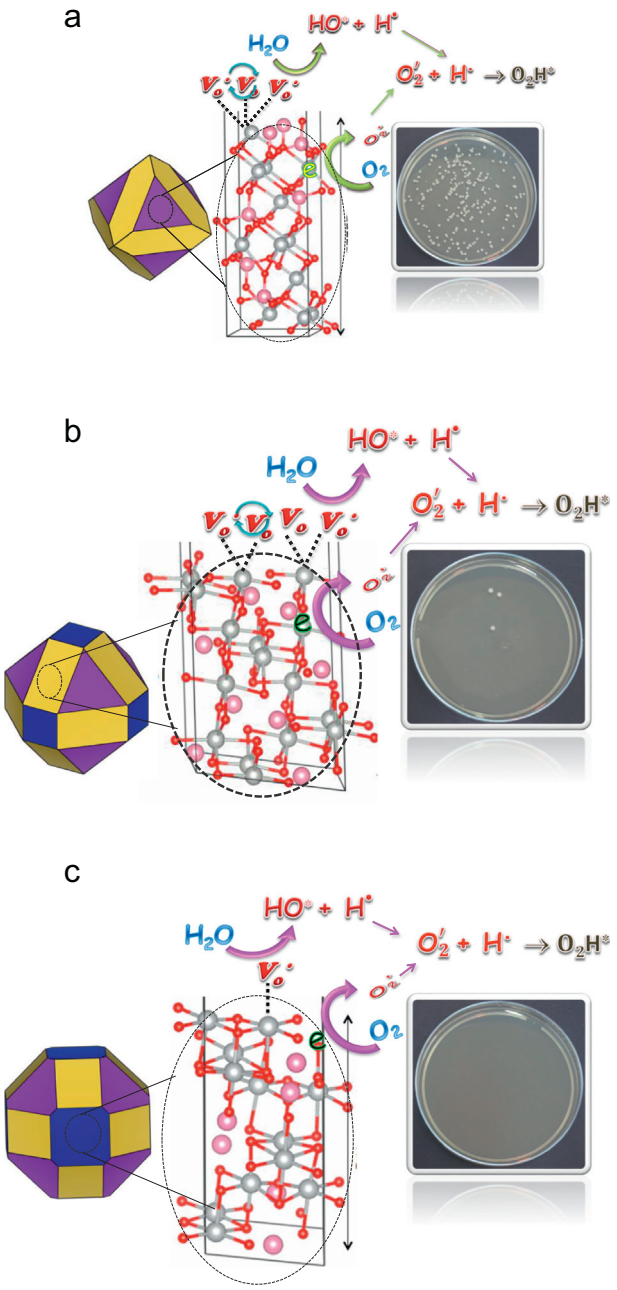

Fig. 6. Mechanism of free radical formation, associated with the predominant face of the β-Ag_2MoO_4 crystal obtained in (a) water, (b) ammonia, and (c) ethanol.

hole for water, which decomposes into a hydroxyl radical and a proton (OH* and H•). Simultaneously, $[AgO_4V_O^xV_O^{\bullet}]$, $[AgO_3V_O^{\bullet}V_O^{\bullet}V_O^{\bullet\bullet}]$, $[AgO_3V_O^xV_O^{\bullet}V_O^{\bullet}]$, $[AgO_4V_O^xV_O^{\bullet\bullet}]$,$[MoO_4]_O'$, and $[AgO_6]'$transfer an electron to the oxygen molecule (O_2), which produces O_2' that interacts with the proton and forms the O_2H^* radical. Fig. 6a, b, and c illustrate the formation of these radicals.

According to the Wulff crystal representation of the optimized β-Ag_2MoO_4 (Fig. 4), and the FE-SEM images presented in Fig. 3, when β-Ag_2MoO_4 is synthetized using water, ammonia, and ethanol as the solvents, the morphologies 1, 2, and 3, respectively, are preferably obtained. This change of morphology is accompanied by the appearance of the (001) surface. When water is used as the solvent, this face is not present. However, when ammonia is used as a solvent, the (001) surface appears in the morphology. Finally, for the microcrystals synthesized in ethanol, this surface becomes more apparent. The results of the microbiological tests (MIC/MBC values and Fig. 5) revealed that the antibacterial efficiency of theβ-Ag_2MoO_4 microcrystals varied with the solvent used in the synthesis, and increased in the following order: water < ammonia < ethanol. Because the appearance of the (001) surface increased the antibacterial efficiency, we propose that the observed mechanism of β-$Ag_2MoO_4$for the inactivation of the MRSA and *E. coli* was mainly caused by the presence of the $[AgO_5.\ V_O^x]$ complex clusters.

In the $[AgO_4V_O^xV_O^{\bullet}]$ and $[AgO_3V_O^xV_O^xV_O^{\bullet}]$/$[AgO_3V_O^xV_O^{\bullet}V_O^{\bullet}]$clusters, internal electron-hole recombination can occur, while in the $[AgO_5V_O^{\bullet}]$ complex clusters, the vacancy is separated from the electron because the electron is located in an $[AgO_6]$'organized complex cluster. This justifies the fact that the $[AgO_5V_O^{\bullet}]$ complex clusters are more reactive and thus more effective for antibacterial applications.

Moreover, according to the Wulff crystal representation of optimized β-Ag_2MoO_4, which is shown in Fig. 4, these faces have low surface energy (E_{suf} = 1.28 J/m^2), as determined by the *ab initio* calculations. Therefore, they are more easily polarized, and able to generate OH*, O_2', and O_2H^*, which are responsible for cell death.

3. Conclusion

We established a facile approach for the synthesis of β-Ag_2MoO_4 microcrystals with different morphology by means of the co-precipitation method and by using three different solvents (water, ammonia, and ethanol). All products exhibited powerful bactericidal capability against gram-positive bacteria, namely, MRSA, and gram-negative bacteria, namely, *E. coli*. The biocidal power increased in the following order: water < ammonia < ethanol. The relationship between the morphology of the differentβ-Ag_2MoO_4 microcrystals synthesized with different solvents, and their biological effect, was constructed systematically by combining experimental techniques and first-principle calculations. The morphologies were calculated by the Wulff crystal constructions based on first principle calculations using three surfaces: (001), (111), and (011). It was concluded that, morphologically, the larger presence of the (001) surface enhanced the antibacterial activity against the MRSA and *E. coli* bacteria. We are firmly convinced that the present study opens up the possibility for extensive investigation, not only for antimicrobial activity, but also for other applications such as the photocatalytic activity of β-Ag_2MoO_4, which can be controlled by tuning their morphology. Additionally, we expect that the results and concepts presented in this work can be extrapolated to the morphology-controlled synthesis of other materials.

CRediT authorship contribution statement

Camila Cristina De Foggi: Conceptualization, Methodology, Investigation, Formal analysis, Writing - original draft, Writing - review & editing, Visualization. **Regiane Cristina De Oliveira**: Methodology, Investigation, Writing - original draft. **Marcelo Assis**: Methodology, Investigation, Writing - original draft, Writing - review & editing, Visualization. **Maria Tereza Fabbro**: Methodology. **Valmor Roberto Mastelaro**: Methodology, Investigation. **Carlos Eduardo Vergani**: Conceptualization, Validation, Writing - original draft, Writing - review & editing, Supervision. **Lourdes Gracia**: Methodology, Investigation. **Juan Andrés**: Writing - original draft, Writing - review & editing, Supervision. **Elson Longo**: Writing - original draft, Writing - review & editing, Supervision, Funding acquisition. **Ana Lucia Machado**: Conceptualization, Validation, Writing - original draft, Writing - review & editing, Supervision, Funding acquisition, Project administration.

Acknowledgment

The authors are grateful to Fundação de Amparo à Pesquisa do Estado de São Paulo (FAPESP-*Centro de Desenvolvimento de Materiais*

Funcionais: 2013/07296-2 and FAPESP 2015/03654-7), Conselho Nacional de Desenvolvimento Científico e Tecnológico (CNPq 304190/2013-6) and Coordenação de Aperfeiçoamento de Pessoal de Nível Superior (CAPES) (for financially supporting this research). J.A. acknowledges the following Spanish research funding institutions: *PrometeoII*/2014/022 and ACOMP/2015/1202 projects (Generalitat-Valenciana), Ministerio de Economia y Competitividad (CTQ2015-65207-P), Programa de Cooperación Científíca con Iberoamerica (Brasil) of Ministerio de Educación (PHBP14-00020), and Ministerio de Economia y Competitividad, "Salvador Madariaga" program, PRX15/00261.

Appendix A. Supplementary data

Supplementary data to this article can be found online at https://doi.org/10.1016/j.msec.2020.110765.

References

[1] V.D. Araújo, R.L. Tranquilin, F.V. Motta, C.A. Paskocimas, M.I.B. Bernardi, L.S. Cavalcante, J. Andres, E. Longo, M.R.D. Bomio, Effect of polyvinyl alcohol on the shape, photoluminescence and photocatalytic properties of PbMoO4 microcrystals, Mater. Sci. Semicond. Process. 26 (2014) 425–430, https://doi.org/10.1016/j.mssp.2014.05.027.

[2] M. Lei, C.X. Ye, S.S. Ding, K. Bi, H. Xiao, Z.B. Sun, D.Y. Fan, H.J. Yang, Y.G. Wang, Controllable route to barium molybdate crystal and their photoluminescence, J. Alloys Compd. 639 (2015) 102–105, https://doi.org/10.1016/j.jallcom.2015.03.108.

[3] G. da S. Sousa, F.X. Nobre, E.A. Araújo Júnior, J.R. Sambrano, A. dos R. Albuquerque, R. dos S. Bindá, P.R. da C. Couceiro, W.R. Brito, L.S. Cavalcante, M.R. de M.C. Santos, Hydrothermal synthesis, structural characterization and photocatalytic properties of β-Ag2MoO4 microcrystals: correlation between experimental and theoretical data, Arab. J. Chem. 13 (1) (2018) 2806–2825.

[4] R.H.N. Frazão, D.G. Della Rocca, S.M. de Amorim, R.A. Peralta, C.D. Moura-Nickel, A. de Noni Jr., R. de F.P.M. Moreira, Plastic optical fibres applied on the photocatalytic degradation of phenol with Ag2MoO4 and ß-Ag2MoO4/Ag3PO4 under visible light, Environ. Technol. (2019) 1–12.

[5] P.P. George, N. Devanna, G. Apsana, An efficient Sonochemical technique for situ coating of Ag2MoO4 nanoparticles on silver and copper beads, J. Bionanoscience. 12 (2018) 854–858.

[6] S.K. Meena, N.L. Heda, G. Arora, L. Meena, B.L. Ahuja, Performance of hybrid exchange-correlation potential for photocatalytic silver chromate and molybdate: LCAO theory and Compton spectroscopy, Phys. B Condens. Matter 560 (2019) 236–243.

[7] W. Du, L. Liu, K. Zhou, X. Ma, Y. Hao, X. Qian, Black lead molybdate nanoparticles: facile synthesis and photocatalytic properties responding to visible light, Appl. Surf. Sci. 328 (2015) 428–435, https://doi.org/10.1016/j.apsusc.2014.12.068.

[8] D. Zhang, R. Zhang, C. Xu, Y. Fan, B. Yuan, Microwave-assisted solvothermal synthesis of nickel molybdate nanosheets as a potential catalytic platform for NADH and ethanol sensing, Sensors Actuators B Chem. 206 (2015) 1–7, https://doi.org/10.1016/j.snb.2014.09.013.

[9] B.K. Maji, H. Jena, R. Asuvathraman, K.V.G. Kutty, Electrical conductivity and thermal expansion behavior of MMoO4 (M = Ca, Sr and Ba), J. Alloys Compd. 640 (2015) 475–479, https://doi.org/10.1016/j.jallcom.2015.04.054.

[10] Z. Du, H. Zhao, C. Yang, Y. Shen, C. Yan, Y. Zhang, Optimization of strontium molybdate based composite anode for solid oxide fuel cells, J. Power Sources 274 (2015) 568–574, https://doi.org/10.1016/j.jpowsour.2014.10.062.

[11] B. Senthilkumar, R.K. Selvan, D. Meyrick, M. Minakshi, Synthesis and characterization of manganese molybdate for symmetric capacitor applications, Int. J. Electrochem. Sci. 10 (2015) 185–193.

[12] M. Najafi, A. Abbasi, M. Masteri-Farahani, V.H.N. Rodrigues, Synthesis, characterization and crystal structure of a copper molybdate coordination polymer as an epoxidation catalyst, Inorganica Chim. Acta. 433 (2015) 21–25, https://doi.org/10.1016/j.ica.2015.04.030.

[13] K.A. Bhabu, S.R. Balaji, R. Sree Devi, T. Balu, G. Muralidharan, T.R. Rajasekaran, Investigations on growth and characterization of glycine admixture sodium molybdate crystals for nonlinear optical applications, Optik (Stuttg) 127 (2016) 1708–1713, https://doi.org/10.1016/j.ijleo.2015.11.134.

[14] C.H.B. Ng, W.Y. Fan, Uncovering metastable α-Ag2MoO4 phase under ambient conditions. Overcoming high pressures by 2, 3-Bis (2-pyridyl) pyrazine doping, Cryst. Growth Des. 15 (2015) 3032–3037.

[15] V. Kumar, S. Matz, D. Hoogestraat, V. Bhavanasi, K. Parida, K. Al-Shamery, P.S. Lee, Design of Mixed-Metal Silver Decamolybdate Nanostructures for high specific energies at high power density, Adv. Mater. 28 (2016) 6966–6975, https://doi.org/10.1002/adma.201601158.

[16] E. Liu, W. Wang, Y. Gao, J. Jia, Tribological properties of adaptive Ni-based composites with addition of lubricious Ag2MoO4 at elevated temperatures, Tribol. Lett. 47 (2012) 21–30, https://doi.org/10.1007/s11249-012-9958-z.

[17] T. Zhang, C. Huang, H. Lan, L. Du, W. Zhang, Tribological properties and lubrication mechanisms of a Ag–Mo composite, Lubr. Sci. 28 (2016) 141–156, https://doi.org/10.1002/ls.1306.

[18] R. Sundaram, K.S. Nagaraja, Solid state electrical conductivity and humidity sensing studies on metal molybdate–molybdenum trioxide composites (M = Ni2+, Cu2+ and Pb2+), Sensors Actuators B Chem. 101 (2004) 353–360, https://doi.org/10.1016/j.snb.2004.04.005.

[19] S. Misra, V. Jayaraman, T. Gnanasekaran, Electrical conductivity and ammonia sensing characteristics of nanocrystalline silver molybdates synthesized by solution chemistry route, 2011 Int. Conf. Nanosci. Technol. Soc. Implic. 2011, pp. 1–6, , https://doi.org/10.1109/NSTSI.2011.6111791.

[20] Z.Y. Bao, D.Y. Lei, J. Dai, Y. Wu, In situ and room-temperature synthesis of ultralong Ag nanoparticles-decorated Ag molybdate nanowires as high-sensitivity SERS substrates, Appl. Surf. Sci. 287 (2013) 404–410 https://doi.org/10.1016/j.apsusc.2013.09.167.

[21] E.K. Fodjo, D.-W. Li, N.P. Marius, T. Albert, Y.-T. Long, Low temperature synthesis and SERS application of silver molybdenum oxides, J. Mater. Chem. A 1 (2013) 2558–2566, https://doi.org/10.1039/C2TA01018F.

[22] A.F. Gouveia, J.C. Sczancoski, M.M. Ferrer, A.S. Lima, M.R.M.C. Santos, M.S. Li, R.S. Santos, E. Longo, L.S. Cavalcante, Experimental and theoretical investigations of electronic structure and photoluminescence properties of β-Ag2MoO4 microcrystals, Inorg. Chem. 53 (2014) 5589–5599, https://doi.org/10.1021/ic500335x.

[23] H. Jiang, J.-K. Liu, J.-D. Wang, Y. Lu, X.-H. Yang, Thermal perturbation nucleation and growth of silver molybdate nanoclusters by a dynamic template route, CrystEngComm 17 (2015) 5511–5521, https://doi.org/10.1039/C5CE00039D.

[24] M. Pandiri, R. Velchuri, R. Gundeboina, V. Muga, A facile in-situ hydrothermal route to construct a well-aligned β-Ag2MoO4/g-C3N4 heterojunction with enhanced visible light photodegradation: mechanistic views, J. Photochem. Photobiol. A Chem. 360 (2018) 231–241, https://doi.org/10.1016/j.jphotochem.2018.04.036.

[25] M. Wu, H. Lv, T. Wang, Z. Ao, H. Sun, C. Wang, T. An, S. Wang, Ag2MoO4 nanoparticles encapsulated in g-C3N4 for sunlight photodegradation of pollutants, Catal. Today 315 (2018) 205–212, https://doi.org/10.1016/j.cattod.2018.01.019.

[26] Y. Li, R. Jin, X. Fang, Y. Yang, M. Yang, X. Liu, Y. Xing, S. Song, In situ loading of Ag2WO4 on ultrathin g-C3N4 nanosheets with highly enhanced photocatalytic performance, J. Hazard. Mater. 313 (2016) 219–228, https://doi.org/10.1016/j.jhazmat.2016.04.011.

[27] J. Li, F. Liu, Y. Li, Fabrication of an Ag/Ag2MoO4 plasmonic photocatalyst with enhanced photocatalytic performance for the degradation of ciprofloxacin, New J. Chem. 42 (2018) 12054–12061, https://doi.org/10.1039/C8NJ02327A.

[28] Z. Jiao, Z. Liu, Z. Ma, Rodlike AgI/Ag2Mo2O7 Heterojunctions with enhanced visible-light-driven photocatalytic activity, ACS Omega 4 (2019) 7919–7930, https://doi.org/10.1021/acsomega.9b00806.

[29] A. Abulizi, K. Kadeer, L. Zhou, Y. Tursun, T. Dilinuer, In situ anion exchange synthesis of β-Ag2MoO4/AgBr heterojunctions with enhanced photocatalytic activity and stability, J. Taiwan Inst. Chem. Eng. 88 (2018) 243–251.

[30] D.W.R. Coimbra, F.S. Cunha, J.C. Sczancoski, J.F.S. de Carvalho, F.R.C. de Macêdo, L.S. Cavalcante, Structural refinement, morphology and photocatalytic properties of β-(Ag 2− 2x Zn x) MoO 4 microcrystals synthesized by the sonochemical method, J. Mater. Sci. Mater. Electron. 30 (2019) 1322–1344.

[31] Y.V.B. De Santana, J.E.C. Gomes, L. Matos, G.H. Cruvinel, A. Perrin, C. Perrin, J. Andrès, J.A. Varela, E. Longo, Silver molybdate and silver tungstate Nanocomposites with enhanced photoluminescence, Nanomater. Nanotechnol. 4 (2014) 22, https://doi.org/10.5772/58923.

[32] S.K. Gupta, P.S. Ghosh, K. Sudarshan, R. Gupta, P.K. Pujari, R.M. Kadam, Multifunctional pure and Eu3+ doped β-Ag2MoO4: photoluminescence, energy transfer dynamics and defect induced properties, Dalt. Trans. 44 (2015) 19097–19110, https://doi.org/10.1039/C5DT03113C.

[33] X. Cui, S.-H. Yu, L. Li, L. Biao, H. Li, M. Mo, X.-M. Liu, Selective synthesis and characterization of single-crystal silver molybdate/tungstate nanowires by a hydrothermal process, Chem. – A Eur. J. 10 (2004) 218–223, https://doi.org/10.1002/chem.200305429.

[34] G. Nagaraju, G.T. Chandrappa, J. Livage, Synthesis and characterization of silver molybdate nanowires, nanorods and multipods, Bull. Mater. Sci. 31 (2008) 367–371, https://doi.org/10.1007/s12034-008-0057-6.

[35] J.C. Sczancoski, M.D.R. Bomio, L.S. Cavalcante, M.R. Joya, P.S. Pizani, J.A. Varela, E. Longo, M.S. Li, J.A. Andrés, Morphology and blue photoluminescence emission of PbMoO4 processed in conventional hydrothermal, J. Phys. Chem. C 113 (2009) 5812–5822, https://doi.org/10.1021/jp810294q.

[36] D.P. Singh, B. Sirota, S. Talpatra, P. Kohli, C. Rebholz, S.M. Aouadi, Broom-like and flower-like heterostructures of silver molybdate through pH controlled self assembly, J. Nanopart. Res. 14 (2012) 781, https://doi.org/10.1007/s11051-012-0781-0.

[37] M.T. Fabbro, C.C. Foggi, L.P.S. Santos, L. Gracia, A. Perrin, C. Perrin, C.E. Vergani, A.L. Machado, J. Andrés, E. Cordoncillo, E. Longo, Synthesis, antifungal evaluation and optical properties of silver molybdate microcrystals in different solvents: a combined experimental and theoretical study, Dalt. Trans. 45 (2016) 10736–10743, https://doi.org/10.1039/C6DT00343E.

[38] F.S. Cunha, J.C. Sczancoski, I.C. Nogueira, V.G. de Oliveira, S.M.C. Lustosa, E. Longo, L.S. Cavalcante, Structural, morphological and optical investigation of β-Ag2MoO4 microcrystals obtained with different polar solvents, CrystEngComm 17 (2015) 8207–8211, https://doi.org/10.1039/C5CE01662B.

[39] C. Bréchignac, P. Cahuzac, N. Kebaili, A. Lando, A. Masson, M. Schmidt, Synthesis of silver molybdate clusters driven by laser-annealing, J. Chem. Phys. 121 (2004) 9617–9622, https://doi.org/10.1063/1.1805497.

[40] C.A. Oliveira, D.P. Volanti, A.E. Nogueira, C.A. Zamperini, C.E. Vergani, E. Longo, Well-designed β-Ag2MoO4 crystals with photocatalytic and antibacterial activity, Mater. Des. 115 (2017) 73–81, https://doi.org/10.1016/j.matdes.2016.11.032.

[41] Z. Li, X. Chen, Z.-L. Xue, Microwave-assisted hydrothermal synthesis of cube-like

Ag-Ag2MoO4 with visible-light photocatalytic activity, Sci. China Chem. 56 (2013) 443–450, https://doi.org/10.1007/s11426-013-4845-5.
[42] C.H.B. Ng, W.Y. Fan, Crystal origami: preparation of β-Ag2MoO4 concave and convex crystals with high-index facets, ChemNanoMat 3 (2017) 178–182, https://doi.org/10.1002/cnma.201600362.
[43] J. Davies, D. Davies, Origins and evolution of antibiotic resistance, Microbiol. Mol. Biol. Rev. 74 (2010) 417–433.
[44] M.T. Fabbro, C. Saliby, L.R. Rios, F.A. La Porta, L. Gracia, M.S. Li, J. Andrés, L.P.S. Santos, E. Longo, Identifying and rationalizing the morphological, structural, and optical properties of β-Ag2MoO4 microcrystals, and the formation process of Ag nanoparticles on their surfaces: combining experimental data and first-principles calculations, Sci. Technol. Adv. Mater. 16 (2015) 65002, , https://doi.org/10.1088/1468-6996/16/6/065002.
[45] J.V. Kumar, R. Karthik, S.-M. Chen, V. Muthuraj, C. Karuppiah, Fabrication of potato-like silver molybdate microstructures for photocatalytic degradation of chronic toxicity ciprofloxacin and highly selective electrochemical detection of H 2 O 2, Sci. Rep. 6 (2016) 34149.
[46] J. Andrés, M.M. Ferrer, L. Gracia, A. Beltran, V.M. Longo, G.H. Cruvinel, R.L. Tranquilin, E. Longo, A combined experimental and theoretical study on the formation of Ag filaments on β-Ag2MoO4 induced by electron irradiation, Part. Part. Syst. Charact. 32 (2015) 646–651, https://doi.org/10.1002/ppsc.201400162.
[47] M.A. Wikler, Methods for dilution antimicrobial susceptibility tests for bacteria that grow aerobically: approved standard, CLSI. 26 (2006) M7–A7.
[48] A.J.F. Egan, R.M. Cleverley, K. Peters, R.J. Lewis, W. Vollmer, Regulation of bacterial cell wall growth, FEBS J. 284 (2017) 851–867, https://doi.org/10.1111/febs.13959.
[49] W. Jiang, A. Saxena, B. Song, B.B. Ward, T.J. Beveridge, S.C.B. Myneni, Elucidation of functional groups on gram-positive and gram-negative bacterial surfaces using infrared spectroscopy, Langmuir 20 (2004) 11433–11442.
[50] T. Shiraishi, S. Yokota, S. Fukiya, A. Yokota, Structural diversity and biological significance of lipoteichoic acid in Gram-positive bacteria: focusing on beneficial probiotic lactic acid bacteria, Biosci. Microbiota, Food Heal. 35 (2016) 147–161, https://doi.org/10.12938/bmfh.2016-006.
[51] O.K. Dalrymple, E. Stefanakos, M.A. Trotz, D.Y. Goswami, A review of the mechanisms and modeling of photocatalytic disinfection, Appl. Catal. B Environ. 98 (2010) 27–38, https://doi.org/10.1016/j.apcatb.2010.05.001.
[52] Y. Li, W. Zhang, J. Niu, Y. Chen, Mechanism of photogenerated reactive oxygen species and correlation with the antibacterial properties of engineered metal-oxide nanoparticles, ACS Nano 6 (2012) 5164–5173, https://doi.org/10.1021/nn300934k.